SSRG International Journal of Electrical and Electronics Engineering
ISSN: 2348-8379/ https://doi.org/10.14445/23488379/IJEEE-V10I1P101

Volume 10 Issue 1, 1-14, January 2023

Original Article

Hybrid Energy System for Smart DC Microgrid Using Optimized PI-Based CUK Integrated Boost DC-DC Converter

Yannam Ravi Sankar[1], K. Chandra Sekhar[2]

[1]*Department of Electrical and Electronics Engineering, Dr. YSR ANUCET, Guntur, Andhra Pradesh, India.*
[2]*Department of Electrical and Electronics Engineering, RVR & JC College of Engineering, Guntur, India.*

[1]*Corresponding Author : yannamraviisankar@gmail.com*

Received: 20 November 2022 Revised: 01 January 2023 Accepted: 10 January 2023 Published: 29 January 2023

Abstract *- In this research work, an efficient DC microgrid is designed with a combination of a fuel cell, a PV system and a battery to improve the system voltage stability. For the purpose of raising the low DC output voltage of the PV system, a Cuk integrated converter is used, and a crew search optimized Proportional Integral (PI) controller is used to regulate a converter's operations to produce a regulated output. Fuel's low DC output voltage is increased by implementing a boost converter, and a PI controller regulates the functioning of the converter to produce a regulated output. Since the output of solar PV systems and fuel cells is influenced by the availability of sunlight and hydrogen, a suitable storage battery is necessary to store the excess electricity generated. The Lithium-ion (Li-ion) battery acts as a power reserve, maintains energy balance, and enhances the power supply reliability of hybrid energy systems. The bidirectional converter, which connects the battery to the Microgrids, has the ability to transfer power in both directions and supports both buck and boost operational parameters. Bidirectional converter is operated under the control of an artificial neural network (ANN). The findings are generated by verifying the suggested method using MATLAB simulation.*

Keywords *- Cuk integrated boost converter, ANN, CSA, Lithium-ion battery, PI controller, Bidirectional converter, DC microgrid, PV system, Fuel cell.*

1. Introduction

Microgrids are local distribution networks made up of a number of loads, energy storage devices and distributed generation units. The microgrid is operated in two modes: 1) grid-tied mode (infused to the power grid) and 2) Islanded mode (isolated from the power grid). When the fault occurs, the microgrids ensure a smooth transition to islanded mode from grid-tied mode [1]. Some of the most significant benefits offered by microgrids are power quality improvement, system reliability and security [2]. There are three types of microgrids in general: AC, DC and hybrid microgrids (integration of both DC and AC microgrids). Compared to an AC microgrid, a DC microgrid has gained more importance owing to several benefits it provides, including a simple design, the requirement of only a few parameters to control, and ease of installation and integration. An AC microgrid, in contrast, necessitates extra factors like frequency synchronization and reactive power control, making the control algorithm very difficult to compute.

Even though AC micro-grid benefits by using the existing ac-power grids, control approaches, protection measures and standards, it suffers from power quality and stability issues. Electronic power converters are used in DC microgrids to connect energy storage systems, AC/DC loads, and renewable energies to the same DC bus. Maintaining DC bus voltage stability and regulating power sharing is difficult for DC microgrids. [3-5].

To fulfil the massive growth in electric power requirement and minimize the use of fossil fuels that results in pollution issues, integration of RESs into the electrical power system is highly indispensable. Hydropower, fuel cells, Photovoltaic (PV), geothermal and wind are some examples of renewable energy sources used to generate electricity [6,17,30]. Solar PV systems have increased drastically because of the abundant availability of sunlight and the shortage of fossil fuels like coal, natural gas, etc. Additionally, the solar PV system contributes to limiting global warming by emitting no greenhouse gas emissions. [7]. To increase the low output voltage provided by solar panels and to obtain controlled output under various climatic and solar irradiation conditions, a DC-DC converter with high voltage gain is essential [8, 9]. Converters like the Cuk converter [10], zeta converter [11], boost converter [12], SEPIC converter [33], buck-boost converter [14], Luo converter [15] and others are used to regulate power generation so that solar energy can be harvested to its full potential.

The conventional PI controller regulates DC quantities, enhances the PV grid-tied system's dynamic operation and has a simple design, so it is considered the preferable controller in PV grid-connected systems.

Although it effectively controls the DC variables, it has many flaws, including non-zero and steady-state error, procedure failure all through load variations, and finding the optimal Controller gains values is challenging because of the nonlinearity of PV systems and their fluctuating characteristics. Conventional approaches, such as trial and error, take more time and produce errors when it comes to tuning PI parameters. On the other hand, metaheuristic algorithms have been used to acquire precise PI parameters owing to their simple design, easy implementation and absence of derivatives [16, 34]. Ant Colony Optimization (ACO) [18], Particle Swarm Optimization (PSO) [19], Harmony Search Algorithm (HSA) [20] and other metaheuristic algorithms are utilized to optimize the PI controller. A fuel cell is a device which performs electrochemical energy conversion and generates electric current when fuel and oxidant are supplied.

It uses hydrogen or simple hydrocarbon as fuel to produce direct electric current and gives out heat and water as by-products [22,32]. A battery is always directly connected to a DC bus in a conventional solar power generation system. The battery is subjected to a certain potential risk when the load changes abruptly without proper current control. In this instance, a bidirectional converter connects the battery to the DC bus to regulate a decreasing current. [23]. In a microgrid, Battery Energy Storage Systems (BESSs) are considered critical components as they enhance power quality and reliability, maintain energy balance and prevent energy loss. The battery stores the required amount of electrical energy when there is surplus energy generation and supplies the excess energy to the grid and load whenever necessary [24, 25,27].

This study proposes a hybrid energy system with a hydrogen-based fuel cell, a PV system, and a storage battery coupled to Microgrids. The incorporation of primary energy sources such as Fuel cells and PV to the DC microgrid is achieved using a boost converter and Cuk integrated boost converter, respectively. The DC bus interfacing of the Li-ion battery, considered a backup source, is accomplished by applying a bidirectional converter. An operation of Cuk integrated boost converter, boost converter, and bidirectional converter are enhanced by using crow search optimized PI controller, PI controller and ANN controller, respectively. The battery operates as an energy buffer, controlling the power flow by executing charging and discharging operations. The results are obtained after the verification of the proposed method using MATLAB simulation.

2. Literature Review

A [26,31] nonlinear non-affine dynamic model was used to construct the DC microgrid. Two nonlinear control strategies are suggested to achieve voltage regulation based on a non-affine control input model. Nonlinear regulation-based control offers the potential to use fewer states to regulate the system, providing further cost, reliability, and resilience benefits. Passivity-based control necessitates each state to be available to control throughout the operation. However, it faces challenges like computational tractability and mitigating complexity.

In [31] to improve DC-bus voltage regulation and preserve power balance, a nonlinear ITSMC) utilizing a modified regulation rule is presented. It has been demonstrated that the suggested reaching law's reaching time is shorter than the standard attaining time for the same gain value and suitable for different operating conditions. However, parallel multi-solar PV converters' reliability and smooth switching are crucial and fail in solving parametric uncertainties.

In [28], a power management strategy was proposed for a DC-linked HMG to operate economically and intelligently. It was proven through rigorous testing that HMG employs the suggested scheme intelligently by adjusting to the varied operating circumstances. Despite its advantages, it shows degraded performance towards the system.

In [29], a grid-tied DC microgrid system was examined utilizing PV and wind power generation and constant power loads, resistors and grid-connected VSC. This research examines and improves system stability under significant CPL absorption and inadequate AC grid settings. However, more stabilization is required for continuous system operation and improved system stability.

In [21, 35], an unsatisfactory solution for the class of DC MG with a nonlinear, non-affine dynamic model was found using the SDRE technique. The transient performance of the SDRE regulator is assessed under illumination and load variation, and the results demonstrate a significant improvement. Despite its merits, significant improvement in the controller is required for satisfactory nonlinear structures.

3. Proposed system

As indicated in Figure 1, the fuel cell/PV system and storage battery compensate the hybrid power plant for a DC microgrid linked to this study research. Power generation systems, Li-ion batteries, and the central DC microgrid are all connected using DC-DC power conversions. The Cuk integrated boost converter is incorporated to enhance PV panel output. An error signal is produced by relating the converter's actual output voltageV_{act}, to an expected reference value V_{ref} . An obtained error signal is processed by the crow search optimized PI controller to provide a reference control signal, which steers the PWM generator to initiate gating pulses. DC-DC Cuk integrated boost converter's switching activity is regulated by the PWM generator's gating pulses, which provide a controlled DC voltage.

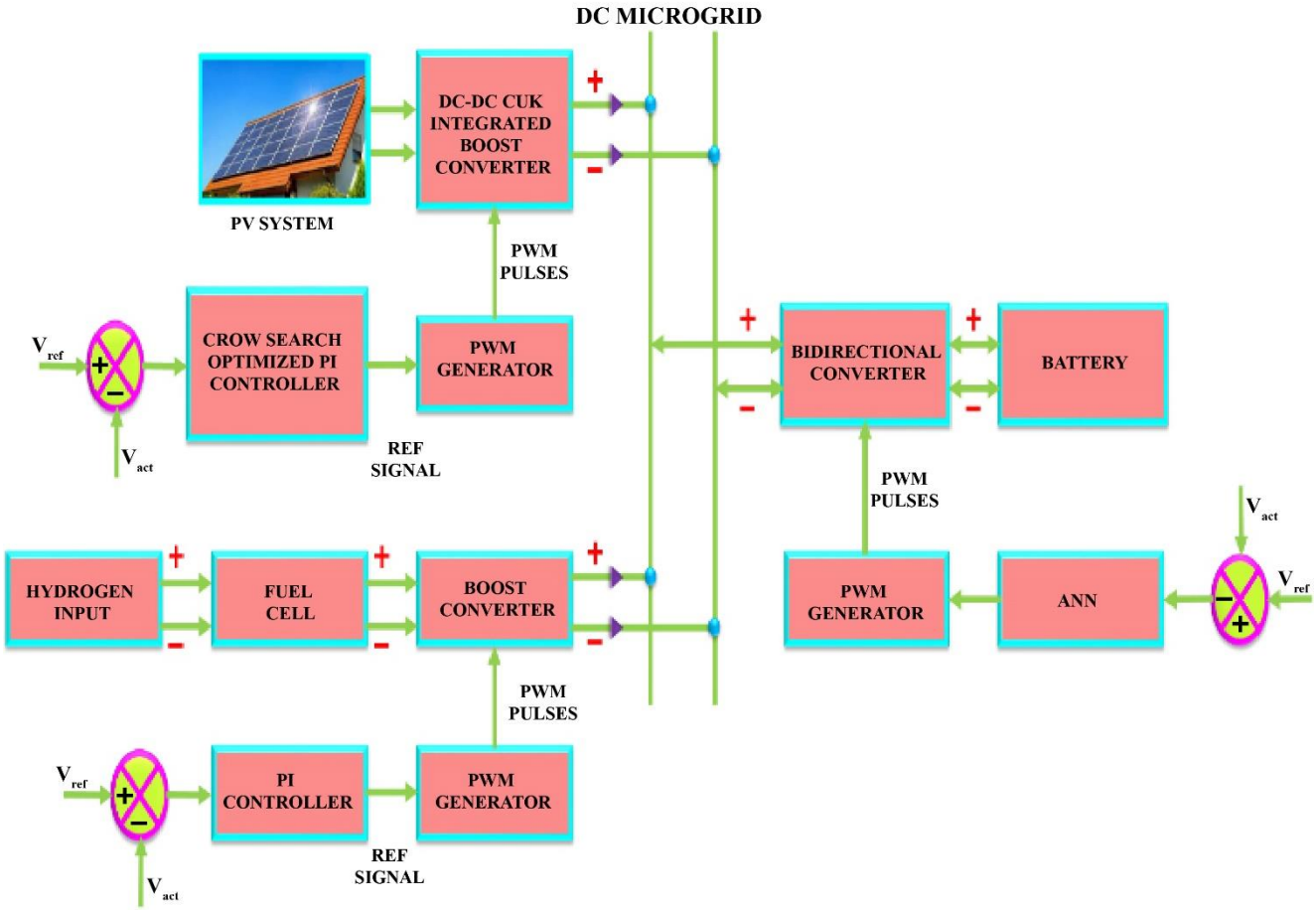

Fig. 1 Proposed hybrid energy system for DC microgrid

When hydrogen fuel is fed to the fuel cell, DC voltage is generated, which is then boosted using a boost converter. The PI controller gives an error signal to the PWM generator by equating the converter's actual DC output voltage V_{act} with reference voltage V_{ref}. The PWM pulses produced by the PWM generator control the boost converter's switching action to provide a controlled DC voltage. In order to store the surplus energy produced, a suitable storage battery is required. This is because fuel cells and solar PV systems can only function while sunlight is present and hydrogen input is available. The battery serves as an energy buffer, which indicates that it performs charging and discharging operations to keep the power flow balanced. The reference voltage V_{ref} and the actual battery voltage V_{act} are compared to get error voltage, which is converted to a control signal using ANN and fed to the PWM generator for the generation of PWM pulses. A bidirectional converter, which is connected to the battery, is controlled by the pulses produced.

4. Proposed system modelling

4.1. Modelling of Solar PV system

A large area pn junction semiconductor diode is essentially what a solar cell is, which is a crucial part of a solar photovoltaic system. The solar cells arranged in the solar panel produce electric current by using a photovoltaic effect when exposed to sunlight. Cells are usually made of semiconductor materials to accomplish effective photovoltaic energy conversion. In a solar cell, the photovoltaic conversion efficiency indicates the ratio of PV electrical power generated to irradiation power. Figure 2 depicts the electrical network setup for the solar cell's equivalents.

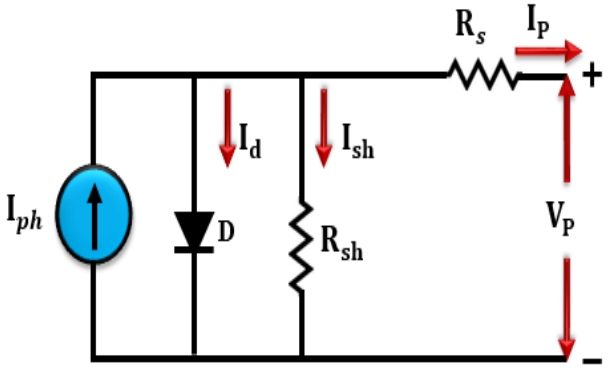

Fig. 2 Solar cell's equivalent electrical network diagram

The parameters of a PV module's current voltage are as follows:

$$I_P = I_{ph} - I_d\left[exp\left(\frac{V_P+I_PR_s}{nv_{te}}\right)-1\right]-\frac{V_P+I_PR_s}{R_{sh}} \quad (1)$$

$$v_{te} = \frac{akT}{q} \quad (2)$$

Where,
I_{Ph} : Photo current in A
I_P : Panel output current in A
V_P : Panel output voltage in V
I_d: Diode saturation current in A
n: Number of series-connected solar cells
R_s : Series resistor in Ω
R_{sh}: Shunt resistor in Ω
v_{te}: Diode thermal voltage in V
k: Boltzmann constant (1.381×10^{-23}J/K)
a: Diode ideality constant
q: Electron charge (1.602×10^{-19} C)
T: The temperature on the absolute scale in K
Open circuit voltage is given as,

$$V_{oc} = \frac{akT}{q} Log_n\left(\frac{I_{ph}}{I_d} + 1\right) \quad (3)$$

An output voltage of the panel is increased by the suggested Cuk integrated boost converter. Utilizing this high voltage gain DC-DC converter minimizes the number of solar panels needed.

4.2. Analysis of Cuk Integrated Boost Converter

Cuk integrated boost converter is a hybrid converter obtained by combining the conventional boost and the Cuk converter, as represented in Figure 3. The arrangement of the input inductor, input source and power switches are similar in both these converters; therefore, integration of these converters is achieved easily by positioning the input inductor and power switch on the input side in common. This hybrid converter offers high voltage gain as it combines the benefits of boost and Cuk converter. The converter utilizes a single switch to facilitate Continuous Current Mode (CCM) operation, which lowers voltage spikes on the diodes and controlled switch.

In terms of voltage gain ratio, the suggested converter performs better than boost and Cuk converters. Figure 4 illustrates the three different operating modes of the Cuk integrated boost converter. The charging as well as discharging derivations of the capacitors and inductors used in this converter are also specified below.

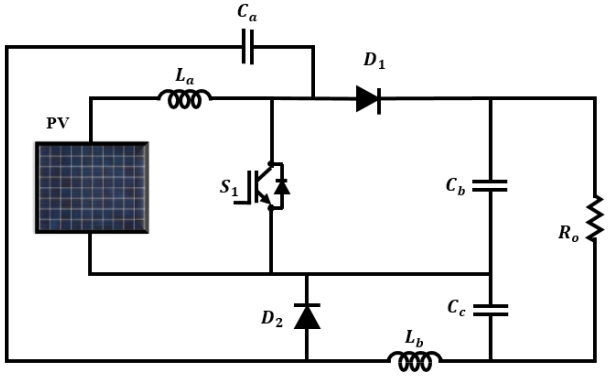

Fig. 3 Cuk integrated boost converter's circuit diagram

4.2.1. Modes of Operation of Cuk integrated Boost converter

Mode 1 $(t_0 - t_1)$

The mode 1 operation begins when t=t_0, the power switch S_1 is switched ON, and the inductors (L_a and L_b) are charged till t_1. During this interval, the capacitor C_a starts discharging through S_1 and negative voltages V_{C_b} and V_{C_a} block diode D_1 and D_2. Here V_{C_b} and V_{C_a} are the voltage across the capacitors C_b and C_a respectively.

Mode 2 $(t_1 - t_2)$

The mode 2 operation is initiated when t=t_1, the power switch S_1 is turned OFF. Here a voltage V_{C_a} is lower than V_{C_b}. During this time interval, the capacitor C_a gets charged, whereas the inductors L_a and L_b get discharged. As diode D_1 is still operating under reverse bias conditions, diode D_2 continues to conduct.

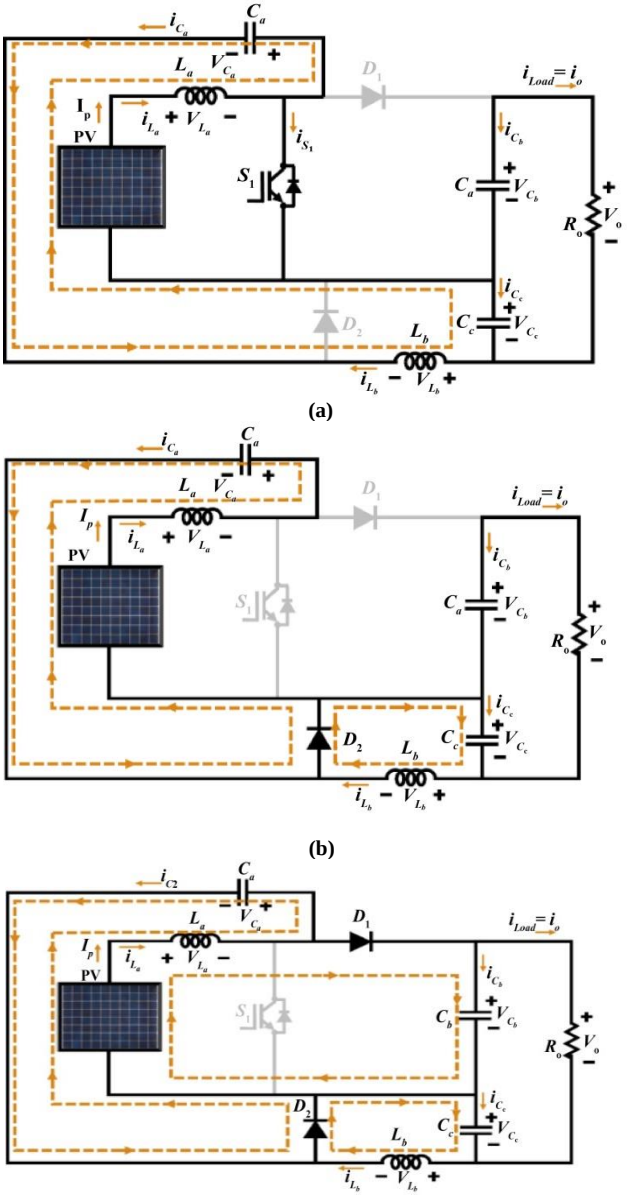

Fig. 4 The operational modes of a Cuk integrated boost converter are: (a) Mode 1, (b) Mode 2 and (c) Mode 3

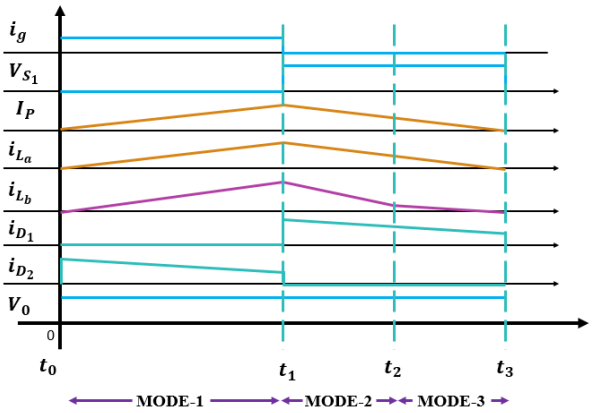

Fig. 5 Proposed converter waveforms

Mode 3 $(t_2 - t_3)$

Here power switch S_1 continues to remain in OFF condition and voltage across the capacitor C_b is equal to or less than the voltage across the capacitor C_a. Inductors L_a and L_b are in discharging mode, whereas capacitors C_b and C_a are in charging mode and get charged through the inductorL_aAs a result, the diodes D_1 & D_2 conduct and current flows through the load. Figure 5 illustrates the proposed converter's waveforms.

Power switch S_1 is turned ON when the converter receives supply voltage V_P from the solar PV system and input current I_P begins to flow. By applying Kirchhoff's voltage law in mode $1(t_0 - t_1)$, capacitor currents $i_{C_a}$and $i_{C_b}$are obtained.

$$-V_P + V_{L_a} = 0 \implies V_{L_a} = V_P \tag{4}$$

$$-V_{C_a} + V_{L_b} + V_{C_c} = 0 \Longrightarrow V_{L_b} = -V_{C_c} + V_{C_a} \tag{5}$$

$$-i_{S_1} + i_{L_a} - i_{C_a} = 0 \tag{6}$$

$$i_0 - i_{L_b} - i_{C_c} = 0 \tag{7}$$

$$i_{C_a} = -i_{L_b} \tag{8}$$

$$i_{C_b} = -i_0 \tag{9}$$

In mode 2 $(t_1 - t_2)$ the operation, the coil delivers energy to the capacitors $C_b$and C_c when the power switch S_1 is turned off. Hence, from loop 1 and loop 2, it is clear that

$$-V_P + V_{L_a} + V_{C_a} = 0 \Longrightarrow V_{L_a} = -V_{C_a} + V_P \tag{10}$$

$$V_{L_b} + V_{C_c} = 0 \Longrightarrow V_{L_b} = -V_{C_c} \tag{11}$$

$$V_{C_a} = V_{C_b} \tag{12}$$

The current flowing through the capacitors $C_b$and C_a are derived by analyzing the loop 1 and loop 2 in mode 2 operation as mentioned below,

$$i_{C_b} = i_{D_1} - i_0 \tag{13}$$

$$i_{C_a} = i_{L_a} - i_{D_1} = i_{D_2} - i_{L_b} \tag{14}$$

The voltage across the capacitors C_b and C_c are derived from equations 15 and 16,

$$\mathrm{V_{C_b}} = \frac{1}{1-\alpha}\mathrm{V_P} \tag{15}$$

$$\mathrm{V_{C_c}} = \frac{\alpha}{1-\alpha}\mathrm{V_P} \tag{16}$$

The converter's output voltage is,

$$V_0 = \frac{1+\alpha}{1-\alpha}V_P \tag{17}$$

Current flowing through an inductor L_a is obtained from the equation given below.

$$V_P i_{L_a} = V_0 i_0 \Rightarrow i_{L_a} = \frac{1+\alpha}{1-\alpha} i_0 \tag{18}$$

The inductors L_a and L_b values are obtained from equations 19 and 20,

$$L_a = \frac{V_P \alpha T}{\Delta i_{L_a}} \tag{19}$$

$$L_b = \frac{V_{C_c}(1-\alpha)T}{\Delta i_{L_b}} \tag{20}$$

The capacitors C_b, C_a and C_c values are calculated from the following equations,

$$C_b = \frac{i_0 \alpha T}{\Delta V_{C_b}} \tag{21}$$

$$C_a = \frac{i_0 \alpha T}{\Delta V_{C_a}} \tag{22}$$

$$C_c = \frac{T \Delta i_{L_b}}{8 \Delta V_{C_c}} \tag{23}$$

4.3. Crow Search Algorithm (CSA)

Askarzadeh proposed the CSA in 2016 as a novel optimization algorithm for finding solutions to problems. Crow is regarded as the smartest bird that usually lives in groups and has a proportionally larger brain than its body size. It maintains a watchful eye on other birds intending to identify the location where the birds store their food and steals it once the owner has left. CSA is a population-based metaheuristic algorithm that draws inspiration from crow flocks' hunting habits.

4.4. Crow Search Optimized PI Controller

The objective function is essential to design an effective crow search optimized PI controller that provides better results when compared to the conventional PI controller. Integral of Square Error (ISE), Integral of Absolute Error (IAE), Time Absolute Error (ITAE) and

Integral of Time Square Error (ITSE) are the four indices commonly used to represent the system performance considering the complete closed-loop response. The single objective function cannot provide the optimal solution for controller optimization. So individual objective functions with proper weights must be integrated to obtain better performance. Crow search optimized PI controller is stimulated for the four multi-objective functions given in the equations below

$$F_1 = B * ISE + (1 - B) * T_S * M_P \quad (24)$$

$$F_2 = B * ITSE + (1 - B) * T_S * M_P \quad (25)$$

$$F_3 = B * IAE + (1 - B) * T_S * M_P \quad (26)$$

$$F_4 = B * ITAE + (1 - B) * T_S * M_P \quad (27)$$

Where, $T_S \rightarrow$ settling time
$M_P \rightarrow$ Maximum overshoot and
$B \rightarrow$ Weighting factor

Input:

Number of iterations ($iter_{max}$)
Awareness Probability (AP)
Crow flock size (N)
Dimensions (d)
Flight length (fl)

4.4.1. Initialization

- Perform the random generation of K_p and K_i values which indicate a preliminary position of N crows in d dimensions.
- Assign the memory of the crows with initial positions.
- Calculate the control system's performance with N different PI controllers based on the fitness function value.
- Use equation (24) – equation (27) for estimating the fitness function (F) and saving the minimum value as f_{min}.
- For i=1:N
- if random ≥ AP
- $K_p^{i,iter+1} = K_p^{i,iter} + random\ value$
- $K_i^{i,iter+1} = K_i^{i,iter} + random\ value$

else

$K_p^{i,iter+1}$ and $K_i^{i,iter+1}$= a random position of search space

End

4.4.2. Calculate

If the PI controller's fitness function value with new positions is found to be better than the previous value,

- Set the [best meal best index] to the minimum (F)
- if the best food is superior than f_{min}
- update K_{pnew}= K_p(best index) and K_{inew}= K_i(best index)
- update memory

$$m^{i,iter+1} = K_{pnew}^{i,iter+1} K_{inew}^{i,iter+1}$$

End

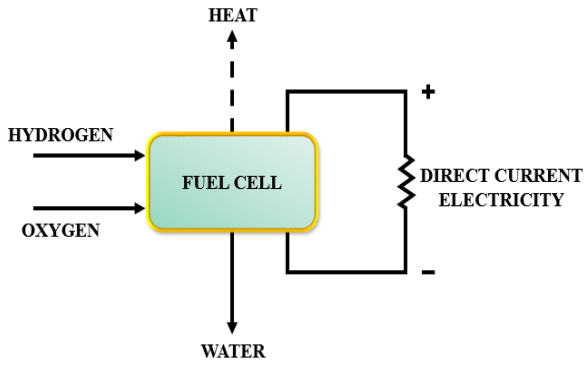

Fig. 6 Hydrogen fuel cell

4.5. Fuel Cell Modelling

When furnished with fuel, a fuel cell generates electricity through an electrochemical energy conversion mechanism. It produces clean energy and has the ability to convert fuel's chemical energy into electrical energy with greater efficacy. It comprises an anode (positive electrode), cathode (negative electrode) and electrolyte. The fuel cell provides noiseless operation due to the absence of moving parts. It's a thermodynamically open system that uses a variety of fuel and oxidant combinations. The fuel cell requires hydrogen as a fuel and oxygen as an oxidant, commonly acquired from the air, to generate direct current, heat and water, as shown in Figure 6. Here anode and cathode are provided with hydrogen and oxygen, respectively. With the assistance of a catalyst, a hydrogen atom ionizes into an electron and a proton and reaches the cathode in two separate paths. The electron reaches the cathode via an electrical circuit, whereas the proton passes through an electrolyte. The fuel cell's kind, the operation temperature, and the catalyst, which speeds up the chemical process, affect how much energy it can create.

The hydrogen gas is ionized at the anode, releasing electrons and producing H^+ions (or protons) as mentioned below. Energy is produced as a result of this reaction.

$$2H_2 \rightarrow 4H^+ + 4e^- \quad (28)$$

Water is created at the cathode when oxygen interacts with H+ ions from the electrolytes and e- ions from the electrodes.

$$O_2 + 4e^- + 4H^+ \rightarrow 2H_2O \quad (29)$$

Through the use of a boost converter, which raises the fuel cell's output voltage level, fuel cells are connected to the DC microgrid.

4.6. Fuel Cell-Based Boost Converter

Boost converter, a step-up converter named for its purpose, is depicted in Figure 7 along with its system design. During steady-state operation, an output voltage V_0 is generally higher than an input voltage V_{dc}. Boost converter embodies a power switch S, an inductor L, a load resistor R along with a filter capacitor C. An inductor

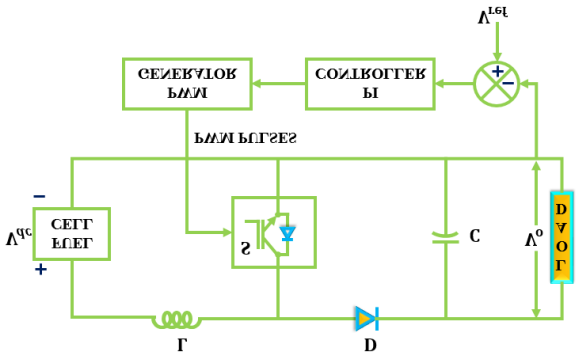

Fig. 7 Circuit diagram of boost converter connected to fuel cell

current waveform, the converter is operated in continuous and discontinuous conduction modes. ON duty ratio $\alpha = \frac{t_{on}}{T}$ is needed to turn the switch S ON and OFF at the switching frequency $f_s = \frac{1}{T}$.

4.6.1. Mode 1

An inductor L, which is connected to the sourceV_{dc}, begins to store energy when power switch S is in an ON state at the time periodt_{on}. Diode D isolates the output stage by operating under reverse bias conditions.

4.6.2. Mode 2

The output stage receives energy from both the inductor and the input when switch S is in an OFF state at the time period t_{off} . Now the current flows through D, L, R, and C. Figure 8 shows the mode 1 and mode 2 operation of the boost converter.

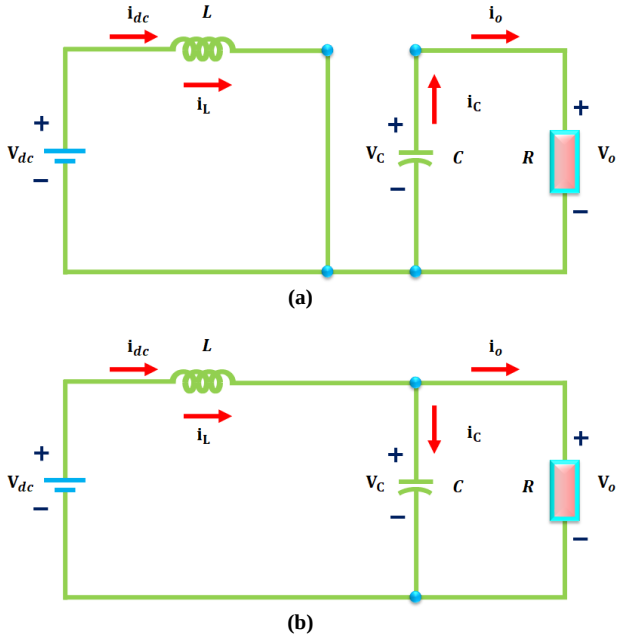

Fig. 8 (a) Mode 1 (switch-on) and (b) Mode 2 (switch-off) of the Boost converter

$$\frac{V_0}{V_{dc}} = \frac{1}{(1-\alpha)} \tag{30}$$

Where V_0 and V_{dc} refers to the converter's output and input voltages, respectively, and α refers to the duty cycle of the power switch.

Value of an inductor is calculated as

$$L = \frac{V_{dc}}{f_s \Delta i_L}\,\alpha \tag{31}$$

$\Delta i_L \rightarrow$ Input current ripple

Equation (32) gives the value of the capacitor C

$$C = \frac{i_0}{f_s \Delta V_0}\,\alpha \tag{32}$$

$\Delta V_0 \rightarrow$ Output voltage ripple

4.7. PI Controller-Based Boost Converter

The PI controller is the most predominantly used conventional controller, which is simple in design and easy to implement. It compares an actual DC output voltage V_{act} of a boost converter with the reference voltage V_{ref} and generate an error (e), which is fed to the PWM generator for generating PWM pulses. The converter's performance is improved because the pulses produced in this way control the converter's switching action. For the sake of processing the error and producing an optimum control (u), this controller performs both proportional and integral actions as mentioned below:

$$u = K_P e + K_I \int e\, dt \tag{33}$$

The process of determining control parameters K_P and K_I to achieve desired performance specifications is known as PI tuning.

4.8. Battery Management System

The Lithium-ion (Li-ion) battery is used as it has high energy density and power density[13]. The important function of the battery is to store excess power generated from both the PV system and the fuel cell. First of all, the error voltage is calculated by simply comparing the actual battery voltage $V_{Battery}$ and the reference voltageV_{ref}. An error voltage is first determined by simply comparing the voltage battery $V_{Battery}$ and reference voltageV_{ref}, respectively. The ANN controller optimizes the error voltage before being fed to the PWM generator, which produces PWM pulses. These pulses alter a power converter's duty cycle and control their switching behaviour to enable the boost and buck types of operations. ANN controller manages its battery's charging and discharging modes to control the power flow direction. Figure 9 presents the power circuit schematic for the battery management system.

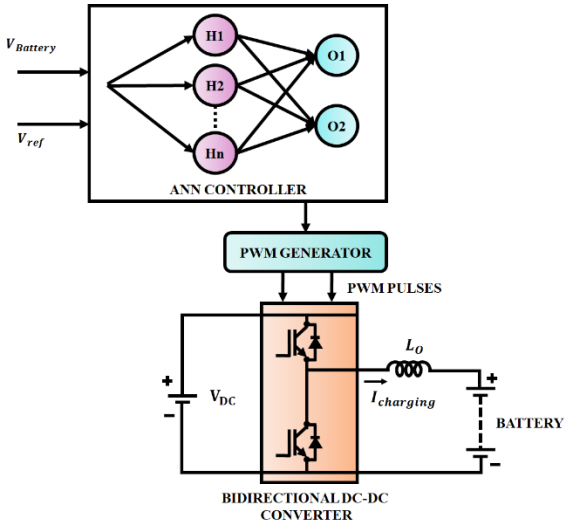

Fig. 9 Power circuit diagram of the battery management system

For the buck mode of operation, equations 34 to 37 are obtained.

$$V_{Battery} = V_{DCLink} - L_O . \frac{dI_{charging}}{dt} \quad (34)$$

$$I_{charging} = \frac{1}{L_O} \int_0^{T_{on}} (V_{DCLink} - V_{Battery}) . dt \quad (35)$$

$$V_{Battery} = -L_O . \frac{dI_{charging}}{dt} \quad (36)$$

$$I_{charging} = \int_{T_{on}}^{T_{off}} \left(-\frac{V_{Battery}}{L_O} \right) . dt \quad (37)$$

For the boost mode of operation, equations 38 to 41 are obtained.

$$V_{Battery} = L_O . \frac{dI_{charging}}{dt} \quad (38)$$

$$I_{charging} = \frac{1}{L_O} \int_0^{T_{on}} (V_{Battery}) . dt \quad (39)$$

$$V_{Battery} + V_{L_O} = V_{DCLink} \quad (40)$$

$$I_{charging} = \frac{1}{L_O} \int_{T_{on}}^{T_{off}} (V_{Battery} + V_{DCLink}) . dt \quad (41)$$

The battery management system is very essential in this hybrid energy system-based DC microgrid for improving power quality, system reliability and maintaining energy balance.

5. Results

This study's main goal is to maintain the DC microgrid's hybrid energy system-based voltage stability. Cuk integrated boost converter and bidirectional converter is employed to integrate the PV system, fuel cell and battery into the DC microgrid, respectively. To improve and regulate DC output voltage, a variety of control approaches are used to regulate the efficiency of DC-DC converters. MATLAB simulation is used to verify the efficiency of this hybrid energy system-based DC microgrid.

Table 1. Solar panel and Fuel cell specifications

Solar panel	
Parameters	Values
Peak power	$2\ kW$
Open circuit voltage V_{OC}	$22.6\ V$
Series connected solar PV cells	36
No. of panels	$250\ W, 8\ panels$
Short circuit current I_{SC}	$20.833\ A$
Short circuit voltage V_{SC}	$12\ V$
Fuel cell (Stack type)	
Output power	$1\ kW$
Output voltage	$90\ V$
Output current	$11.11\ A$

Table 2. Converter specifications

Cuk integrated boost converter	
Parameters	Values
Switching Frequency f_s	$10\ kHz$
L_a, L_b	$3\ mH$
C_a	$570\ \mu F$
C_b, C_c	$2200\ \mu F$
Boost converter	
Switching Frequency f_s	$10\ kHz$
L	$5\ mH$
C	$2200\ \mu F$

Table 1 presents the requirements for solar panels and fuel cells, whereas Table 2 lists the parameters for converters.

Figures 10(a) and 10(b) show the simulated waveforms that specify the solar intensity and temperature fluctuation.

In 0.2 seconds, the temperature decreases from 35°C to 30°C; in 0.3 seconds, the sun's power decreases from 1000W/m2 to 900W/m2. Figure 11 illustrates how solar radiation intensity and temperature changes affect the current of solar panels and the output voltage. After transient changes at 0.2 and 0.3 seconds, the output voltage and current of the solar panel stay constant. A controlled output of $90\ V$ and $10\ A$ is obtained after $0.3\ s$.

After recovering from the effect of operating condition variations at 0.2 and 0.3 seconds, the proposed converter gives a constant voltage of $300\ V$ and current of $3A$ as output with the support of a crow search optimized PI controller. Figure 13 illustrates the fuel cell's output voltage waveform.

Figures 12(a) and (b) respectively demonstrate the output voltage and current waveform of the Cuk integrated boost converter.

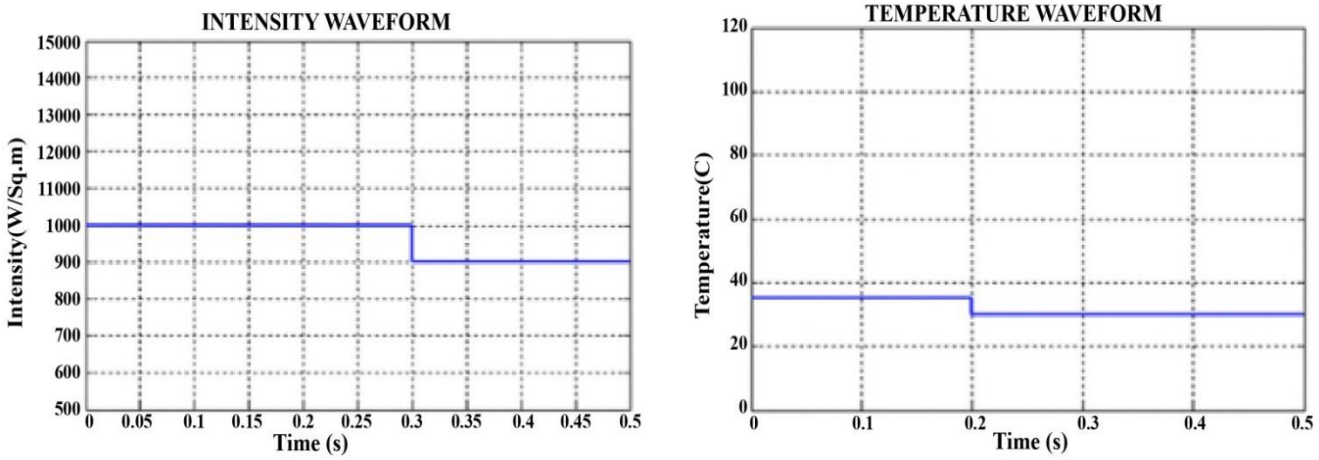

Fig. 10 (a) Solar intensity waveform and (b) Temperature waveform

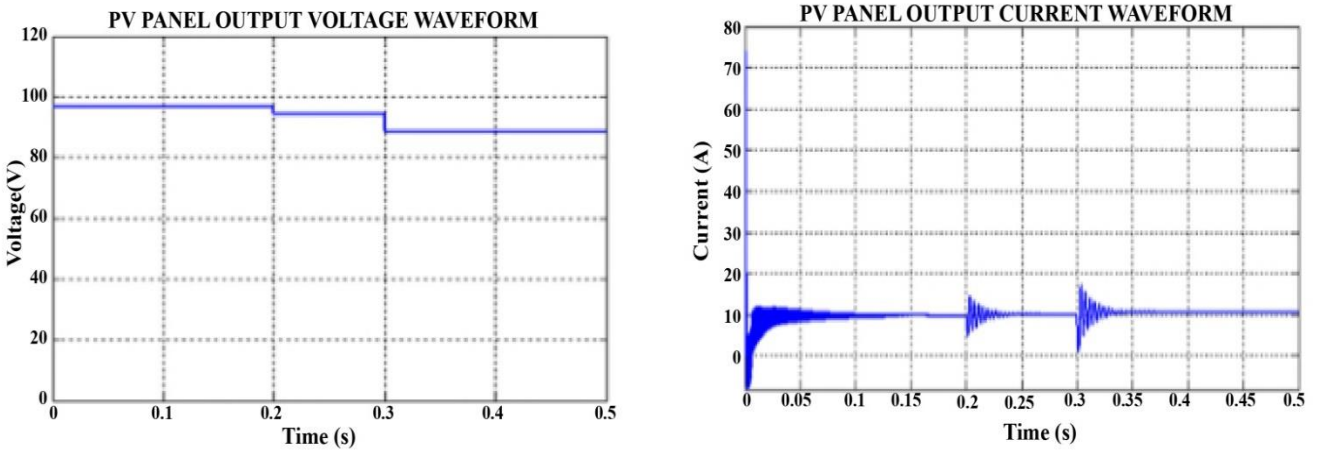

Fig. 11 (a) Output voltage waveform and (b) Output current waveform of PV panel

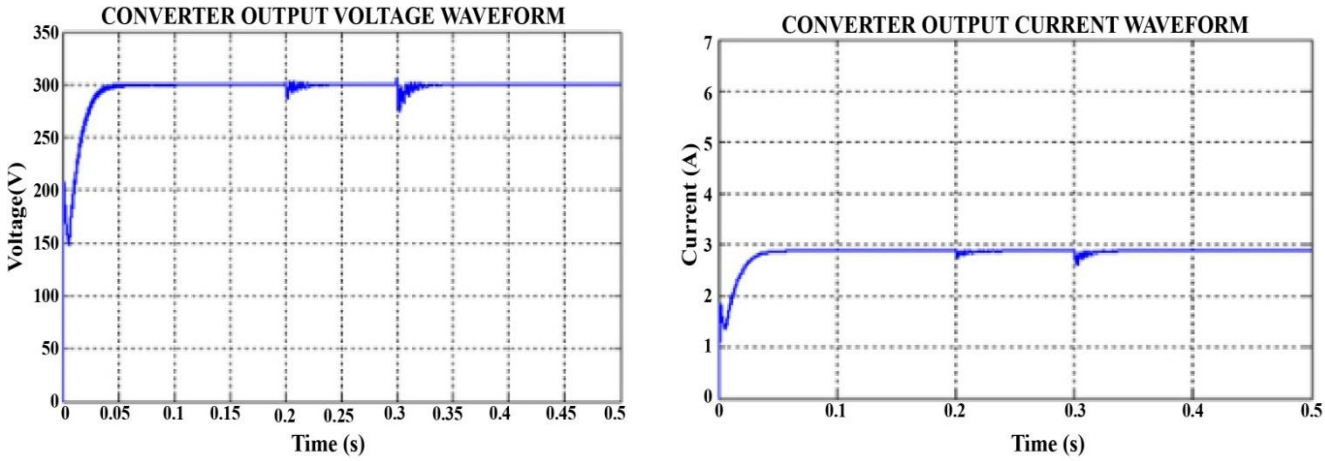

Fig. 12 (a) Converter output voltage waveform (b) Converter output current waveform

Even though the output voltage of the fuel cell varies between $60\,V$ and $120\,V, and$ experiences slight fluctuations; the implementing PI controller helps to mitigate the losses, improve efficiency and ensure controlled output. An output voltage and current waveform of a boost converter connected to a fuel cell are shown in Figure 14.

A PI controller helps the converter produce a constant output of 300 V and 3 A current. Figure 15 represents the solar PV system's input signal and output current.

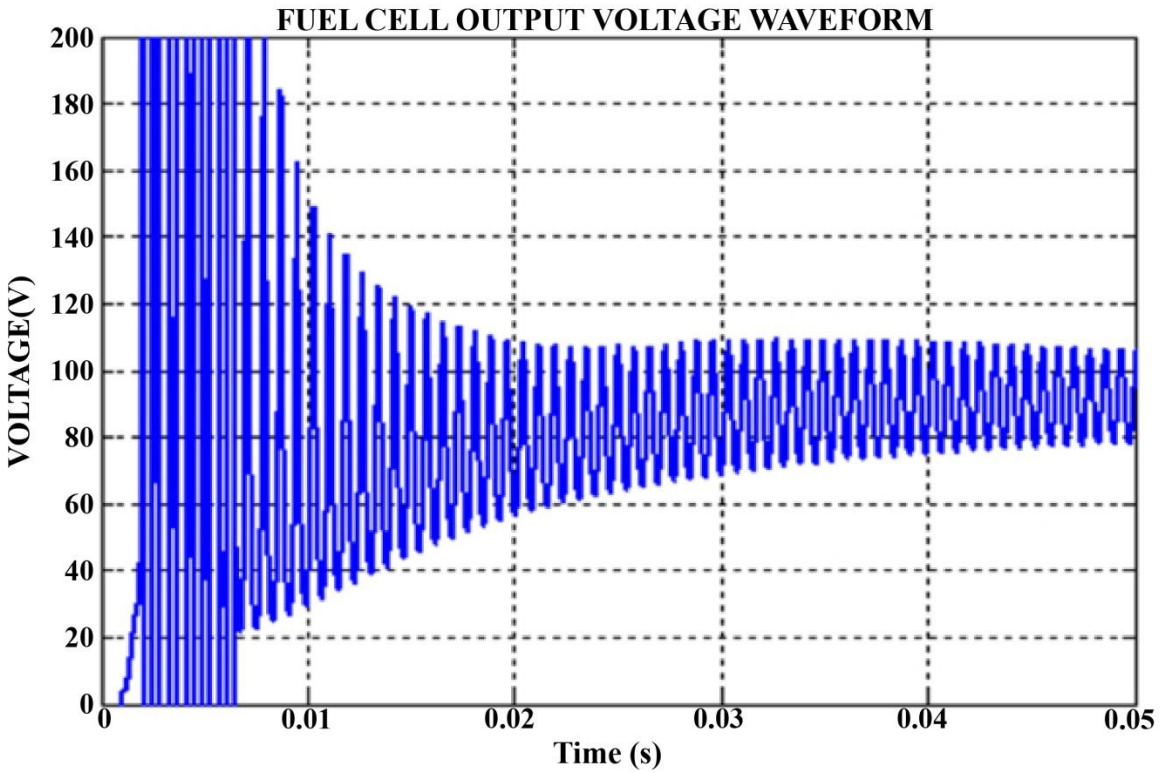

Fig. 13 Fuel cell's output voltage waveform

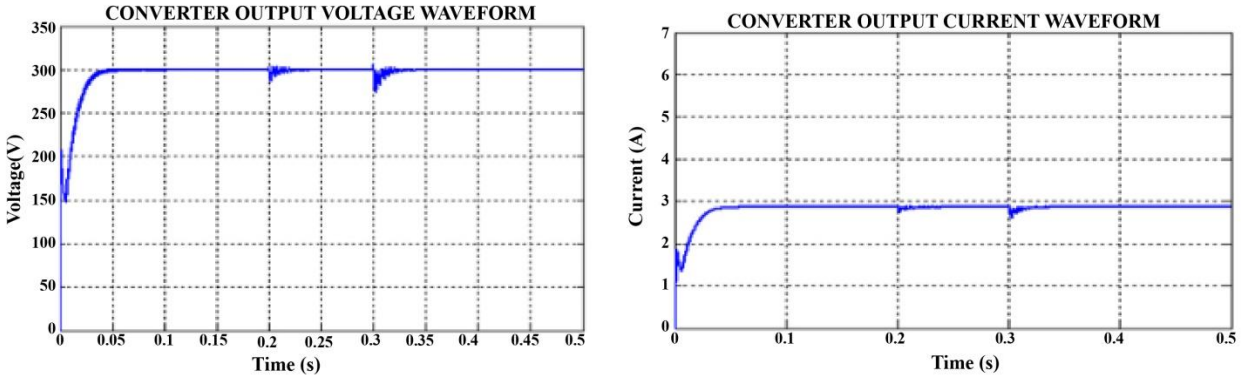

Fig. 14 Converter (a) output voltage waveform and (b) output current waveform

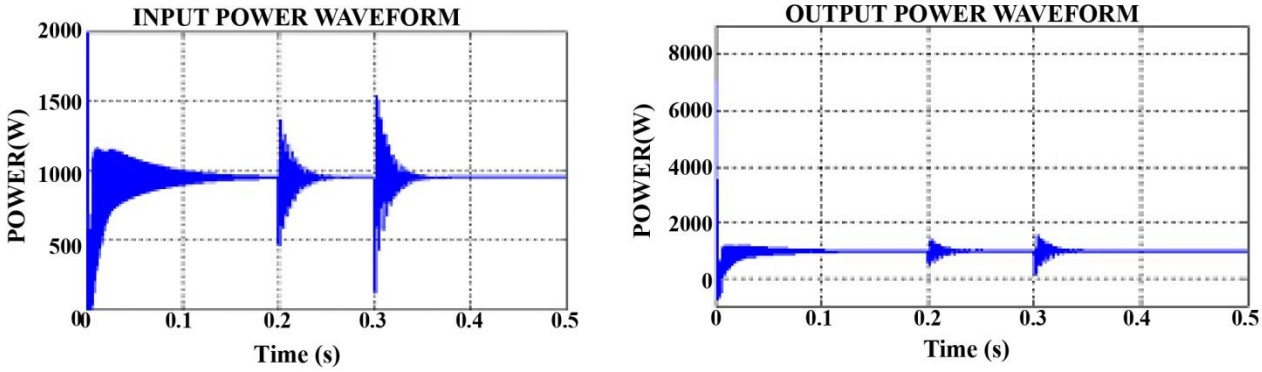

Fig. 15 (a) Input power waveform (b) Output power waveform

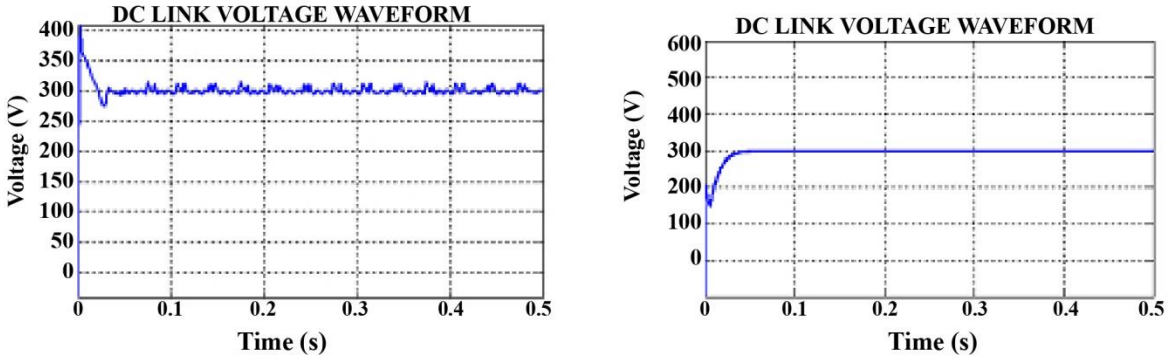

Fig. 16 Comparison of DC link voltage obtained (a) with PI controller and (b) with crow search optimized PI controller

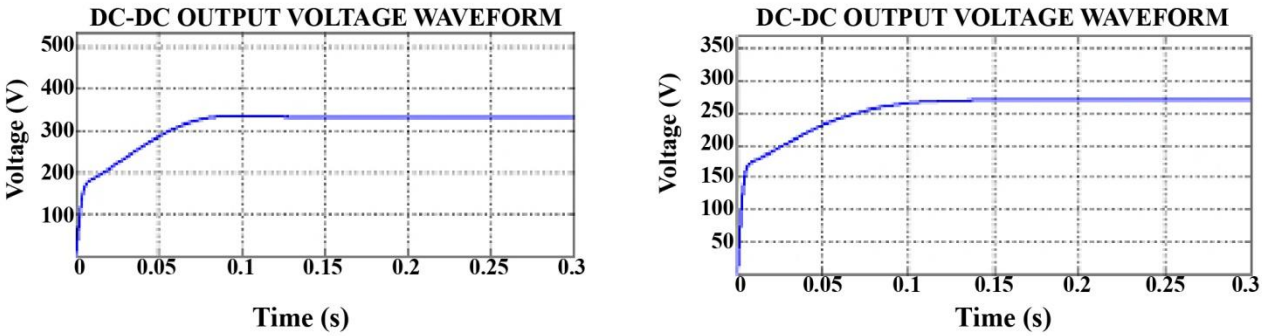

Fig. 17 Output voltage of the converter using crow search optimized PI controller for reference voltages (a) 330 V and (b) 280 V

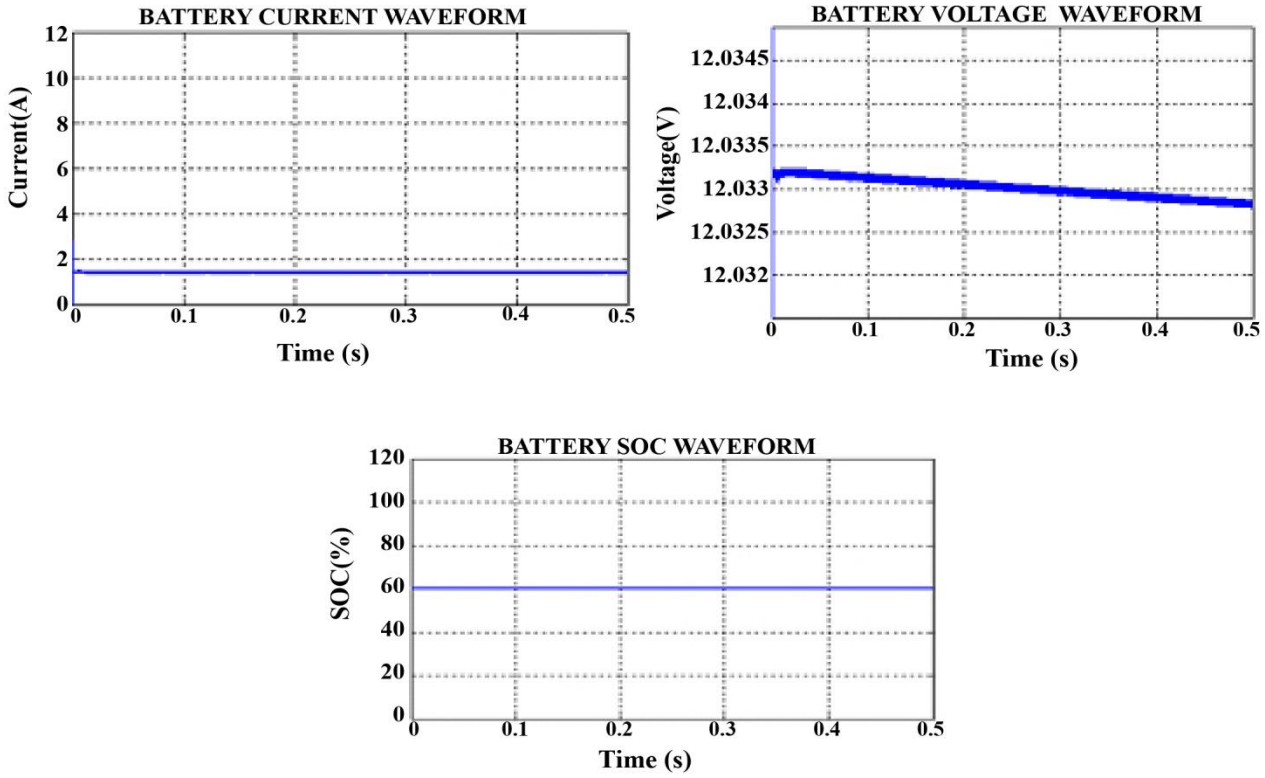

Fig. 18 Battery (a) Current waveform, (b) Voltage waveform and (c) SOC waveform

The input power of the solar panel is around $1000\,W$, whereas the output power is around $940\,W$, which is influenced by temperature and solar insolation variations.

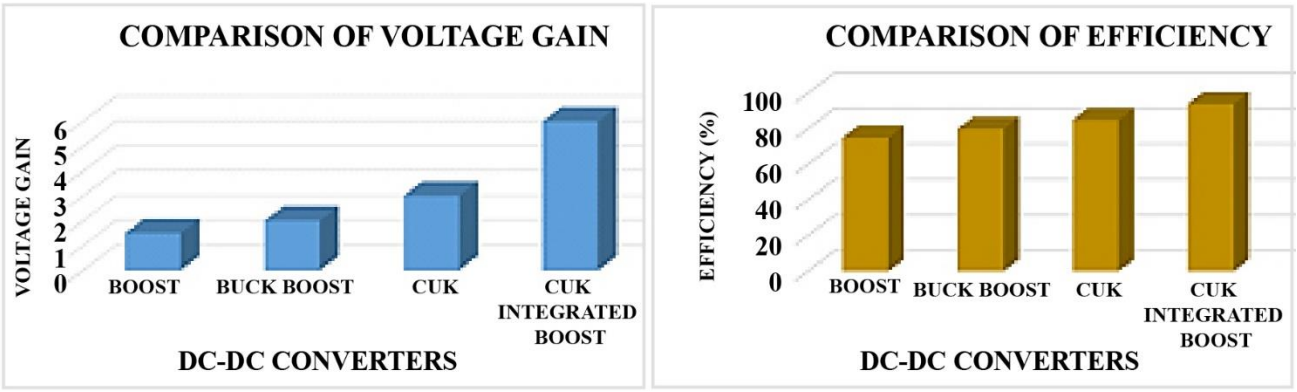

Fig. 19 Comparison of (a) Voltage gain and (b) Efficiency

DC link voltage produced by controlling the converter operation using PI and crow search optimized PI controller is shown in Figure 16. DC link voltage varies, and a stable voltage is not produced when a conventional PI controller controls the converter. By implementing a crow search optimized PI controller, the converter operation is effectively controlled, a constant voltage of 300 V is obtained quickly without fluctuations,s and the settling time is noted at $0.1s$.

Figure 17 illustrates the converter's output voltage using two distinct reference voltages and a crow search-optimized PI controller. It is evident from both output waveforms that peak overshoot problems do not impair the converter's output, which stabilizes at 0.1 seconds. Thus it is concluded that for any reference voltage, a stable and controlled DC voltage output is attained with the proposed control technique.

Figure 18. (a), (b) and (c) show, respectively, the waveforms of the battery's voltage, current and state of charge (SOC).

The State Of Charge (SOC) of a battery is the amount of charge it has with respect to its capacity and is expressed in percentage. The battery is charged when the SOC is below 60% and discharged when the SOC value is above 60%. The voltage lowers marginally even though the battery current remains constant at 1.8 A.

The voltage gain of common converters, including boost, buck-boost, and Cuk converter, is evaluated to Cuk integrated boost converter in Figure 19(a). The Cuk integrated boost converter has a voltage gain ratio of 1:6, which is significantly larger than the voltage gains of the remaining three converters. Boost, Buck-Boost, and Cuk Converter have a voltage gain ratio of 1:1.5, 1:2, and 1:3, respectively. The efficiency of the Cuk integrated boost converter is 94%, as shown in Figure 19(b), which is significantly higher than the efficiency of the other three converters.

6. Conclusion

Changes in load and the intermittent nature of renewable energy sources often impact a microgrid's stability. Proper control of individual renewable energy source, battery and converters interfaced with the DC microgrid enable efficient power distribution and reliable operation. In this proposed system, a fuel cell, a PV system and a storage battery are all connected to the microgrid via a boost converter, Cuk integrated boost converter and a bidirectional converter, respectively. Several control techniques are adopted to control the performance of DC-DC converters and provide higher and controlled DC output voltage. Whenever the primary sources of electricity (photovoltaic and fuel cells) fail to deliver the desired output, the battery provides continuous electricity to the microgrid, whose charging and discharging modes are controlled by the ANN controller. Utilizing MATLAB simulation, the effectiveness of the suggested system is assessed, and results show that the Crow search-optimized PI controller successfully lowers power fluctuations in the hybrid energy system.

References

[1] Ali Hooshyar, and Reza Iravani, "Microgrid Protection," *IEEE*, vol. 105, no. 7, pp. F32-1353, 2017. *Crossref*, https://doi.org/10.1109/JPROC.2017.2669342

[2] Maxx Patterson, N. F. Macia, and A. M. Kannan, "Hybrid Microgrid Model Based on Solar Photovoltaic Battery Fuel Cell System for Intermittent Load Applications," *IEEE Transactions on Energy Conversion.*, vol. 30, no. 1, pp. 359-366, 2015. *Crossref*, https://doi.org/10.1109/TEC.2014.2352554

[3] Yasser Mohammed Alharbi et al., "Super Twisting Fractional Order Energy Management Control for a Smart University System Integrated DC Micro-Grid," *IEEE Access.*, vol. 8, pp. 128692-128704, 2020. *Crossref*, https://doi.org/10.1109/ACCESS.2020.3008858

[4] Masoud Davari, and Yasser Abdel-Rady I. Mohamed, "Robust Multi-Objective Control of VSC-Based DC-Voltage Power Port in Hybrid AC/DC Multi-Terminal Micro-Grids," *IEEE Transactions on Smart Grid*, vol. 4, no. 3, pp. 1597-1612, 2013. *Crossref*, https://doi.org/10.1109/TSG.2013.2249541

[5] Na Zhi et al., "An SOC-Based Virtual DC Machine Control for Distributed Storage Systems in DC Microgrids," *IEEE Transactions on Energy Conversion*, vol. 35, no. 3, pp. 1411-1420, 2020. *Crossref*, https://doi.org/10.1109/TEC.2020.2975033

[6] Mohamed I. Mosaad et al., "Near-Optimal PI Controllers of STATCOM for Efficient Hybrid Renewable Power System," *IEEE Access*, vol. 9, pp. 34119-34130, 2021. *Crossref*, https://doi.org/10.1109/ACCESS.2021.3058081

[7] M. Jedari Zare Zadeh, and S. H. Fathi, "A New Approach for Photovoltaic Arrays Modeling and Maximum Power Point Estimation in Real Operating Conditions," *IEEE Transactions on Industrial Electronics*, vol. 64, no. 12, pp. 9334-9343, 2017. *Crossref*, https://doi.org/10.1109/TIE.2017.2711571

[8] Junfeng Liu et al., "Switched Z-Source/Quasi-Z-Source DC-DC Converters with Reduced Passive Components for Photovoltaic Systems," *IEEE Access*, vol. 7, pp. 40893-40903, 2019. *Crossref*, https://doi.org/10.1109/ACCESS.2019.2907300

[9] Kumaran Nathan et al., "A New DC–DC Converter for Photovoltaic Systems: Coupled-Inductors Combined Cuk-SEPIC Converter," *IEEE Transactions on Energy Conversion*, vol. 34, no. 1, pp. 191-201, 2019. *Crossref*, https://doi.org/10.1109/TEC.2018.2876454

[10] Julio Cezar dos Santos de Morais et al., "Photovoltaic AC Module Based on a Cuk Converter with a Switched-Inductor Structure," *IEEE Transactions on Industrial Electronics*, vol. 66, no. 5, pp. 3881-3890, 2019. *Crossref*, https://doi.org/10.1109/TIE.2018.2856202

[11] Rajan Kumar, and Bhim Singh, "BLDC Motor-Driven Solar PV Array-Fed Water Pumping System Employing Zeta Converter," *IEEE Transactions on Industry Applications*, vol. 52, no. 3, pp. 2315-2322, 2016. *Crossref*, https://doi.org/10.1109/TIA.2016.2522943

[12] Danyang Bao et al., "Switched Inductor Double Switch High Gain DC-DC Converter for Renewable Applications," *IEEE Access*, vol. 9, pp. 14259-14270, 2021. *Crossref*, https://doi.org/10.1109/ACCESS.2021.3051472

[13] Dae-Keun Kang et al., "Selective Recovery of Lithium Sulfate From Spent LFP(Lifepo4) Powder," *International Journal of Engineering Trends and Technology*, vol. 69, no. 11, pp. 122-127, 2021. *Crossref*, https://doi.org/10.14445/22315381/IJETT-V69I11P215

[14] Niraj Rana, and Subrata Banerjee, "Development of An Improved Input-Parallel Output-Series Buck-Boost Converter and Its Closed-Loop Control," *IEEE Transactions on Industrial Electronics*, vol. 67, no. 8, pp. 6428-6438, 2020. *Crossref*, https://doi.org/10.1109/TIE.2019.2938482

[15] Bhim Singh, and Radha Kushwaha, "Power Factor Preregulation in Interleaved Luo Converter-Fed Electric Vehicle Battery Charger," *IEEE Transactions on Industry Applications*, vol. 57, no. 3, pp. 2870-2882, 2021. *Crossref*, https://doi.org/10.1109/TIA.2021.3061964

[16] Fahd A. Alturki et al., "Novel Manta Rays Foraging Optimization Algorithm Based Optimal Control for Grid-Connected PV Energy System," *IEEE Access*, vol. 8, pp. 187276-187290, 2020. *Crossref*, https://doi.org/10.1109/ACCESS.2020.3030874

[17] Deepak Pandey, Manish Khemariya, and Anand Singh, "Performance Analysis of Hybrid Renewable Source RSC-MLC Module Integrated D-STATCOM with PQ Controller," *International Journal of Engineering Trends and Technology*, vol. 70, no. 7, pp. 471-478, 2022. *Crossref*, https://doi.org/10.14445/22315381/IJETT-V70I7P249

[18] Ali Ahmad et al., "Controller Parameters Optimization for Multi-Terminal DC Power System Using Ant Colony Optimization," *IEEE Access*, vol. 9, pp. 59910-59919, 2021. *Crossref*, https://doi.org/10.1109/ACCESS.2021.3073491

[19] Chien-Hung Liu, and Yuan-Yih Hsu, "Design of a Self-Tuning PI Controller for a STATCOM Using Particle Swarm Optimization," *IEEE Transactions on Industrial Electronics*, vol. 57, no. 2, pp. 702-715, 2010. *Crossref*, https://doi.org/10.1109/TIE.2009.2028350

[20] Mir Nahidul Ambia et al., "Harmony Search Algorithm-Based Controller Parameters Optimization for a Distributed-Generation System," *IEEE Transactions on Power Delivery*, vol. 30, no. 1, pp. 246-255, 2015. *Crossref*, https://doi.org/10.1109/TPWRD.2014.2358940

[21] Toqeer Ahmed et al., "Improvement in the Capacity of K-Ion Battery to Supply V-I Capacity in Renewable Technology," *SSRG International Journal of Material Science and Engineering*, vol. 7, no. 3, pp. 1-8, 2021. *Crossref*, https://doi.org/10.14445/23948884/IJMSE-V7I3P101

[22] Xiang Meng et al., "A Dual-Mode Energy Management Strategy Considering Fuel Cell Degradation for Energy Consumption and Fuel Cell Efficiency Comprehensive Optimization of Hybrid Vehicle," *IEEE Access*, vol. 7, pp. 134475-134487, 2019. *Crossref*, https://doi.org/10.1109/ACCESS.2019.2939047

[23] Rui Li, and Fangyuan Shi, "Control and Optimization of Residential Photovoltaic Power Generation System with High Efficiency Isolated Bidirectional DC–DC Converter," *IEEE Access*, vol. 7, pp. 116107-116122, 2019. *Crossref*, https://doi.org/10.1109/ACCESS.2019.2935344

[24] Tingyang Meng, Zongli Lin, and Yacov A. Shamash, "Distributed Cooperative Control of Battery Energy Storage Systems in DC Microgrids," *IEEE/CAA Journal of Automatica Sinica.*, vol. 8, no. 3, pp. 606-616, 2021. *Crossref*, https://doi.org/10.1109/JAS.2021.1003874

[25] Katayoun Rahbar et al., "Energy Cooperation Optimization in Microgrids with Renewable Energy Integration," *IEEE Transactions on Smart Grid*, vol. 9, no. 2, pp. 1482-1493, 2018. *Crossref*, https://doi.org/10.1109/TSG.2016.2600863

[26] Jiwei Sun et al., "Voltage Regulation of DC-Microgrid with PV and Battery," *IEEE Transactions on Smart Grid*, vol. 11, no. 6, pp. 4662-4675, 2020. *Crossref*, https://doi.org/10.1109/TSG.2020.3005415

[27] Himabindu Eluri, and M. Gopichand Naik, "Fractional Order Fuzzy Logic Controller Based Energy Management System for Grid Integrated Microgrid," *International Journal of Engineering Trends and Technology*, vol. 70, no. 5, pp. 227-239, 2022. *Crossref*, https://doi.org/10.14445/22315381/IJETT-V70I5P225

[28] Gopakumar Melath, Sriram Rangarajan, and Vivek Agarwal, "Comprehensive Power Management Scheme for the Intelligent Operation of Photovoltaic-Battery Based Hybrid Microgrid System," *IET Renewable Power Generation*, vol. 14, no. 10, pp. 1688-1698, 2020. *Crossref*, https://doi.org/10.1049/iet-rpg.2019.1368

[29] Hassan Hassantaghi, and Mohsen Rahimi, "Control and Stability Analysis of DC Microgrid System Including Wind and Solar Generation Sources and Grid-Connected Voltage Source Converter," *International Journal of Circuit Theory and Applications*, vol. 49, no. 3, pp. 616-640, 2021. *Crossref*, https://doi.org/10.1002/cta.2948

[30] Chu Donatus Iweh, Semassou Guy Clarence, and Ahouansou H. Roger, "The Optimization of Hybrid Renewables for Rural Electrification: Techniques and the Design Problem," *International Journal of Engineering Trends and Technology*, vol. 70, no. 9, pp. 222-239, 2022. *Crossref*, https://doi.org/10.14445/22315381/IJETT-V70I9P223

[31] Sabrina Yeasmin, Tushar Kanti Roy, and Subarto Kumar Ghosh, "Design of Robust Integral Terminal Sliding Mode Controllers with Exponential Reaching Laws for Solar PV and BESS-Based DC Microgrids with Uncertainties," *Sustainability*, vol. 14, no. 13, pp. 7802, 2022. *Crossref*, https://doi.org/10.3390/su14137802

[32] Jih-Sheng Lai, "Fuel Cell Power Systems and Applications," *IEEE*, vol. 105, no. 11, pp. 2166-2190, 2017. *Crossref*, https://doi.org/10.1109/JPROC.2017.2723561

[33] Kok Soon Tey et al., "Improved Differential Evolution-Based MPPT Algorithm Using SEPIC for PV Systems Under Partial Shading Conditions and Load Variation," *IEEE Transactions on Industrial Informatics*, vol. 14, no. 10, pp. 4322-4333, 2018. *Crossref*, https://doi.org/10.1109/TII.2018.2793210

[34] Sima Seidi Khorramabadi, and Alireza Bakhshai, "Critic-Based Self-Tuning PI Structure for Active and Reactive Power Control of VSCs in Microgrid Systems," *IEEE Transactions on Smart Grid*, vol. 6, no. 1, pp. 92-103, 2015. *Crossref*, https://doi.org/10.1109/TSG.2014.2354651

[35] Mohammad Reza Arabshahi et al., "On the Modelling, Analysis, and Design of a Suboptimal Controller for a Class of Wind/PV/Battery Based DC Microgrid," *IET Renewable Power Generation*, vol. 16, no. 2, pp. 416-434, 2022. *Crossref*, https://doi.org/10.1049/rpg2.12338.